FOREWORD

This report was prepared by the Department of Chemical Engineering and Metallurgy, Syracuse University, Syracuse, New York, under the terms of Contract AF 33(657)-11154. The contract was initiated under Project No. 7350 "Refractory Inorganic Non-Metallic Materials", Task No. 735003 "Refractory Inorganic Non-Metallic Materials; Theory and Mechanical Phenomena". The work was administered under the direction of the Air Force Materials Laboratory, Research and Technology Division, with Mr. Gordon Atkins acting as Project Engineer.

The report covers the performance of work during the period from April 1, 1963 to March 31, 1964.

Acknowledgement is made to C. Chapman, A. Jackson, D. Carlton, C. Chave and L. Barrus for their assistance in the machining of test specimens and the performance of experimental testing.

ABSTRACT

The effect of tensile stress fields due to holes, superimposed on the stress fields due to external notches, was investigated by means of photoelastic techniques and tensile fracture tests. A columbia resin photoelastic material, CR-39, and the titanium alloy 2.5Al-16V, aged to a brittle condition, were used to construct simple model systems for these studies, as a first step to simulate a prototype ceramic material.

For the model systems employed in the investigation, it was found that no significant degree of interaction occurred between the stress fields of holes and the stress field due to the notch. Although the holes produced considerable localized stress inhomogeneities, this effect did not extend to the root of the notch where the maximum stress was solely determined by the stress concentration factor of the notch. The results of the tensile fracture tests confirmed the stress field studies.

It was concluded that elastic stress field equations of notches and holes provide a satisfactory means of estimating the earliest possible interaction of stress raisers. Also, it appears that in a suitable ceramic-prototype there should be an interaction of stress fields extending to locations of maximum stress. It is suggested that this may be achieved by closer spacing and increasing the severity of inhomogeneities.

This technical documentary report has been reviewed and is approved.

W. J. Trapp
Chief, Strength and Dynamics Branch
Metals and Ceramic Division
Air Force Materials Laboratory

TABLE OF CONTENTS

TABLES

ILLUSTRATIONS

INTRODUCTION

The studies described herein were conducted primarily to determine the effects of superimposed stress concentrations in an effort to develop a model for simulating the behavior of technical ceramic materials. This initial program consisted of both theoretical and experimental stress analyses of relatively simple models containing stress concentrations introduced into the models by means of notches and holes.

Materials such as ceramics, ceramoplastics, glasses and certain types of plastics exhibit desirable properties which are attractive for specific service applications. Normally, however, these classes of materials are not seriously considered for critical structural applications, where they are required to support appreciable static loads, because of their known brittle behavior at ambient temperatures. The reasons for this brittle behavior are still somewhat obscure. However, previous studies by the authors (Ref. 1)* concerning the effects of non-uniform stress distribution on the strength of ceramics have provided some insight in this area. As a result of these investigations, it was concluded that fracture in ceramics and similar materials can be analyzed by a maximum fracture stress criterion, provided that material inhomogeneity is also taken into account. It was determined that the fracture of externally notched ceramic specimens was governed by combined effects due to the external notch and the inherent material inhomogeneity.

Thus, the available evidence indicates that ceramics are inhomogeneous materials containing flaws of various sizes in a random distribution throughout the matrix. Such materials are relatively insensitive to the effects of externally introduced stress concentration since they already contain inherent flaws of various severity. Some of the flaws are likely to be more severe than those that can be artificially introduced. Admittedly, this description of ceramics is rather qualitative, at present, and a more detailed study of the interactions between material inhomogeneity and external non-linear stress fields is desirable.

The importance of inhomogeneity and its influence on ceramic material behavior suggests that this characteristic should be more closely examined. Assuming that no bulk plastic flow occurs, and considering a stress concentration type approach, it can be postulated that a homogeneous material may be of two distinct types; namely: (a) a continuous matrix containing no flaws or defects of any kind, and (b) a matrix containing a very large number of very severe flaws. Homogeneous materials of these two types would be expected to exhibit little scatter in mechanical tests on both

*Number in parentheses refer to references at end of manuscript.

Manuscript released by the authors July 1964 for publication as a RTD Technical Documentary Report.

smooth and notched specimens. Obviously, however, the strength of the first type would be considerably higher than that of the second type. Using the same hypotheses, materials in between the two extremes of (a) and (b) would be considered as inhomogeneous and the degree of inhomogeneity would likely depend upon the interaction of several parameters. Examples are materials having a discontinuous matrix, or a continuous matrix containing either a large number of mild flaws or a relatively few number of severe flaws or various combinations of these factors. Thus, flaw density (spacing), flaw severity and the sphere of influence of a given flaw appear to be the controlling parameters that need further study. It was the purpose of the present program to initiate studies in this area.

In the studies described herein, simple model systems were used to determine the stress patterns in the vicinity of artificially introduced flaws (simulated by holes) of various spacings. In addition, the influence of externally introduced stress concentrations (simulated by notches) was examined.

EXPERIMENTAL PROCEDURES

A. Materials

Two different materials were employed in the program; a thermo-setting type plastic known commercially as Homalite "CR-39" and a heat treatable titanium alloy, Ti-2.5Al-16V. The CR-39 was obtained in the form of a 0.25 inch sheet (in 2 lots, designated as lot 1 and lot 2) and the titanium alloy as 0.085 inch sheet. The titanium alloy was received in the solution treated condition and was subsequently aged (after machining of the desired specimens) at 700 F for 4 hours. It was previously shown by Sachs and Sessler (Ref. 2) that Ti-2.5Al-16V, heat treated thusly, will exhibit extremely brittle behavior in the presence of stress concentration. The majority of the experimental tests were conducted on CR-39 to determine the stress distribution due to superimposed stress concentrations by photoelasticity (transmission polariscope) techniques.

B. Test Methods

The investigation consisted primarily of the determination of stress patterns in simple models of CR-39 containing holes and notches of various geometries and spacings. Simple transmission polariscope photoelastic techniques were employed as shown in Figure 1. This arrangement, known as a crossed-circular polariscope, is such that the black isochromatic and colored isochromatic fringes correspond to zero and integral fringe order, respectively.

1. Calibration Tests

In photoelasticity studies, it is important that the fringe constants of the material employed be accurately determined. To accomplish this for CR-39, a calibration procedure was employed using both uniform tension and 4 point load bend tests. The transmission polariscope system of Figure 1 was used for all calibration tests. The calibration specimens are shown in Figure 2. In each calibration, the load-fringe order relationship was observed and recorded and the fringe constants determined from these relationships. The results of the calibration tests in tension are given in Table 1. The data presented in the table are average values of six tests. Load-fringe order (experimental) data showed the predicted linear relation according to

$$\sigma_1 - \sigma_2 = (\text{Fringe constant}) \frac{N}{t} \qquad (1)$$

where N is the observed fringe order and t is the thickness of the specimen (length of optical path).

In uniform tension, $\sigma_2 = 0$ and Equation 1 reduces to

$$\sigma_1 = (\text{Fringe constant}) \frac{N}{t} \qquad (2)$$

The results of the bend calibration tests are also given in Table 1. The fringe constants in the table are the average values of at least five tests. The fringe constants were determined from the equation

$$\text{Fringe constant} = \left(\frac{\sigma_1 - \sigma_2}{N}\right) t = \frac{MCt}{NI} \qquad (3)$$

where M = bending moment
N = moment of inertia
t = specimen thickness
2h = specimen height (See Fig. 2)

The fringe constant values of 82.63 and 92.03, obtained with monochromatic light, were used for the evaluation of subsequent tests on lot 1 and lot 2 material, respectively. These values, obtained from bend tests, are in good agreement with fringe constant values obtained in tension under similar conditions.

2. Shear Stress Distribution Studies in Tension

Edge notch specimens, containing various combinations of small holes in the notched region, were prepared from CR-39 to study the shear stress distribution of these superimposed stress concentrations. The specimen dimensions are given in Table 2 and Figure 3. Notch depth was held constant at about 30 per cent for all specimen designs. The elastic stress concentration factor (Ref. 3) K_t varied from 3 to about 14 by introducing root radii between 0.004 and 0.125 inch. The specimen thickness was kept constant at 0.25 inch. Holes with a diameter of 0.094 inch were spaced between the notch roots, and specimens having equidistant rows of holes were studied, see Figure 3. Unnotched specimens, as shown in Figure 4, were also tested. A stress-strain curve for CR-39 is given in Figure 5.

Shear stress distribution studies were performed using photoelastic techniques. Photographs were taken of the isochromatic patterns produced by applied loads of 105 and 157.7 lbs., respectively. From

these photographs, shear stress was determined from the fringe order distribution measured in the transverse direction from the notch root. Shear stress distribution is obtained by multipling fringe order by the fringe constants as determined by calibration.

3. Tension Tests to Failure

The effect of superimposed stress concentration on notch strength was also studied for the CR-39 specimens described above and on brittle Ti-2.5Al-16V specimens shown in Figure 6. All specimens were tested in a 60,000 lb. capacity Baldwin Universal Testing Machine.

The objective of testing the titanium alloy (in a brittle condition) was to determine the onset of interaction between stress concentrations as a function of their geometry and spacing (ξ). The spacing varied between 0.011 and 0.15 inch.

EXPERIMENTAL RESULTS

A. Shear Stress Distribution Studies in Tension

Photographs of isochromatic patterns of the CR-39 plastic specimens were taken at applied loads of 105 lbs. and 157.7 lbs. By visual analysis, distributions of the isochromatic patterns were measured in the transverse direction between the notch roots. Shear stress distributions were calculated by multipling fringe orders with fringe constants. For the applied load of 105 lbs., the results of studies on all five types of specimens (see Figure 3) are given in Tables 3 and 4 and are illustrated in Figure 7, for all K_t factors included in these studies. The data in Figure 7 is limited to the area in the vicinity of the notch roots. The results for an applied load of 157.7 are given in Tables 5, 6 and 7 and in Figure 8. In Figure 8, the experimental data obtained are compared to theoretical curves of the maximum normal stress, calculated according to Weiss (Ref. 4):

$$\sigma_y = K_t \, \sigma_N \left(\frac{r}{r + 4x}\right)^{1/2} \tag{4}$$

where σ_N = net section stress, r is notch root radius and x is the distance from the notch root. Shear stress distributions, not only in the notched area but across the entire specimen are plotted in Figure 12 at an applied load of 157.7 lbs. for a stress concentration factor of 3.

The theory of photoelastic stress analysis is based on plane stress conditions and the general expressions for Hooke's law are expressed as

$$\epsilon_1 = \frac{\sigma_1}{E} - \frac{\sigma_2}{E}\mu \tag{5}$$

$$\epsilon_2 = \frac{\sigma_2}{E} - \frac{\sigma_1}{E}\mu \tag{6}$$

where σ_1 and σ_2 are the principal stresses
ϵ_1 and ϵ_2 are the principal strains
E is Young's modulus
μ is Poison's Ratio

Therefore

$$\sigma_1 - \sigma_2 = (\epsilon_1 - \epsilon_2)\frac{E}{1+\mu} = 2\tau \tag{7}$$

The principal stress difference $(\sigma_1 - \sigma_2)$ is related to the photoelastic equation

$$\sigma_1 - \sigma_2 = (\text{Fringe Constant})\frac{\text{No. of fringes or fringe order}}{\text{Length of optical path in material}} \tag{8}$$

Thus along every isochromatic fringe the maximum shear stress is constant and is an integral multiple of the shear stress required to produce the first order fringe. The maximum shear stress (τ) can then be calculated from

$$\tau = \frac{\sigma_1 - \sigma_2}{2} \qquad (9)$$

and each isochromatic fringe order corresponds to an integral multiple of 2τ . In addition to the shear stress caused by the applied tensile load, the observed shear stress distributions include residual stresses introduced by machining the photoelastic material. Therefore, assuming that the principal directions of the residual stresses and applied stresses are identical, the observed shear stress is given by

$$2\tau = \sigma_1 - \sigma_2 + 2\tau \text{ residual} \qquad (10)$$

Typical shear stress distribution patterns for various specimen geometries are shown in Figure 10 and sketches of isochromatics for two typical geometries are illustrated in Figure 11. It appears from these figures that, although the holes produce a severe stress inhomogeneity throughout the specimen cross section, the interaction effect in the vicinities of the notch roots or near the holes is hardly noticeable. It also is observed that the maximum shear stress is always at the notch root and that the highest shear stress gradient is in the direction normal to the axis of loading. Minimum shear stress gradients were observed at 10 and 30 degrees for specimen types IV and V and I, II, III, respectively.

B. Results of Tensile Tests to Failure

To study the effect of similated flaws (holes) on the fracture stress, the CR-39 brittle plastic specimens, described previously, were tested to failure in tension. During the tests, the testing machine crosshead speed was held constant at approximately 0.005 in. per min. The results of these tests, based on both nominal and actual net section areas, are given in Table 8 and are illustrated in Figure 9.

Smooth tensile tests were also performed on CR-39 at the same crosshead speed mentioned above, and the results of these tests are also given in Table 8. To check the linear elasticity characteristic of the material, the load-elongation curve was recorded, see Figure 5.

Although it was assumed that CR-39 would behave according to maximum fracture stress concept, the results for Type I specimens (edge-notches only) did not yield the expected ($K_t \sigma_N$ = constant) relationship, see Figure 9. The results of fracture tests on Types II, III, IV and V indicated the same behavior as Type I specimens. In general, however, the Type I specimens

exhibited the highest notch strength at all K_t factors. Thus it appears that the effect of holes and geometrical arrangements is not very pronounced for the geometries studied in this program. This finding is in agreement with the results of the shear stress distribution studies.

Tension tests to failure were also conducted on specimens of Ti-2.5Al-16V sheet (aged to a brittle condition), containing both edge notches and holes. The results of these tests are given in Table 9. The interaction of the notches and holes was not determined quantitatively, but it was observed during the tests that the time delay between crack formation at the notch root and failure of the specimen decreased as the distance between the notch root and the edge of the hole (ξ^e) was increased. Also, based on a limited number of tests, it was found that the fracture strength decreased as the hole was moved closer to the notch root, as shown in Table 9.

DISCUSSION

The experimental results obtained on CR-39 clearly indicate that there is no pronounced interaction between the stress field of holes and that of an edge notch for the geometries investigated. The holes did not affect the magnitude of the maximum stress at the notch root nor the fracture strength of edge notched specimens. Although the holes produce considerable localized stress inhomogeneities, this effect does not extend to the stress distribution near the edge notch. This is clearly seen in Figure 8 and is also demonstrated by the fracture test results where only a very small effect due to hole distribution and hole spacing was noticed.

Theoretical estimates of the stress distribution due to notches and the effect of superimposed holes may be made on the basis of an approximate stress distribution proposed by Weiss. These calculations show that the effect of the stress concentration due to a hole under a stress field of σ_N has diminished to almost zero at a distance of 0.26 in., the closest hole spacing selected for the present investigation. Thus, there was no noticeable interaction to be expected on theoretical grounds between the notch stress field and the hole stress field as confirmed by the experimental results. Consequently, it may be concluded that estimates of the elastic stress distribution based on the Neuber equations, constitutes a safe upper bound for estimating the incidence of interaction. It may be an extremely safe upper bound as is evidenced from the results shown in Figures 7 and 8 which also show the estimated stress distribution, since the actual distribution has a much steeper gradient than the estimated distribution. This is in part due to the increase from zero to a maximum of the second stress, σ_2 normal to the direction of loading in this region. However, this second stress can only account for part of the observed increase in stress gradient.

A rather disturbing feature of the experimental results is the fact that there is considerable disagreement between the theoretical predicted stress concentration factor and the experimentally observed stress concentration factor. In each case, the latter extrapolates to considerably higher values than would be predicted from Neuber's equations. Part of this discrepancy may be due to the residual machining stresses introduced in the production of the notch. More detailed studies of the actual stress distribution in the close vicinity of a notch are required to resolve this dilemma.

A selected number of brittle Ti-2.5Al-16V specimens were tested for which a small hole was introduced as close as possible to the root of a notch. The results, shown in Table 9, indicate that there is some interaction present for the two closest hole spacings of 0.011 and 0.025 in. However, the three data points obtained from this study are hardly sufficient to present a quantitative analysis of the phenomenon.

From the above discussion it is evident that future research in this area, aimed at simulating prototype ceramic materials, will require more complex configurations of superimposed notches and holes or flaws to an extent where actual interaction of the stress fields of the various stress raisers occurs.

In addition, it appears that not only is it necessary to have interaction between the various stress fields of the stress raisers introduced but to also have competing interaction, i.e. several points in the test specimen geometry where a maximum stress similar to that at the root of the notch is obtained. For the present test series this was not the case and the stress at the root of the external edge notch was always the maximum stress. In order to obtain significant interaction it will be necessary to test considerably larger test specimens so that small holes, producing measurable stress fields, can be brought close to rather mild notches. Later on, the internal flaws, as now represented by drilled holes, may have to be replaced by actual flaws, notches or cracks in order to raise their stress concentration factor and obtain competing points of high stress throughout the entire specimen geometry.

SUMMARY AND CONCLUSIONS

A photoelastic study of the effect of the stress field due to multiple holes superimposed on the stress field of edge notches revealed no significant degree of interaction at the points of maximum stress of either stress raiser for the test specimen geometries investigated. For each specimen, the maximum stress occurred at the root of the notch and was unaffected by the presence of a hole 0.260 inch. away from the notch root. Estimates of the degree of interaction with the help of an approximate stress distribution lead to the same results, although, the actually observed stress gradients seem to be higher than those predicted by the approximate elastic stress distribution. Thus, the stress distribution inhomogeneities introduced by the additional holes did not lead to a significant change in the location or magnitude of maximum stress points.

These results are confirmed by fracture tests conducted on the same CR-39 specimens chosen for the stress field study. The net section stress at fracture was almost unaffected by the presence of holes within the selected geometrical distribution, and was primarily determined by the value of the elastic stress concentration factor.

Some interaction with noticeable effects on the fracture strength of brittle titanium was achieved as the notch to hole distance was reduced to 0.011 and 0.025 inch, respectively.

It may thus be concluded that the elastic stress field equations of notches and holes provide a good means of estimating the earlies possibility of interaction between the effects of several stress raisers. Since the stress gradient observed in finite samples is somewhat higher than that predicted by theory for infinitely wide samples, actual interaction may only occur at somewhat closer spacings. Furthermore, it appears that in a suitable ceramic-prototype there must be both interaction of stress fields as well as a competition for stress maxima. This may be achieved by closer spacing of inhomogeneities and a raising of the stress concentration factor of these inhomogeneities.

REFERENCES

1. Weiss, V., Sessler, J. G., Grewal, K. and Chait, R., "The Effect of Stress Concentration on the Fracture and Deformation Characteristics of Ceramics and Metals", ASD-TDR-63-380, (April 1963).

2. Sachs, G. and Sessler, J. G., "Effect of Stress Concentration on Tensile Strength of Titanium and Steel Alloy Sheet at Various Temperatures", ASTM STP No. 287, Symposium on Low Temperature Properties of High Strength Aircraft and Missile Materials, (1960).

3. Peterson, R. E., "Stress Concentration Design Factors", John Wiley and Sons, New York, N. Y., (1953).

4. Weiss, V., "Application of Weibull's Statistical Theory of Fracture To Sheet Specimens", ASME Paper No. 62-WA-270, (November 1962).

5. Neuber, H., "Kerbspannungslehre", Springer-Verlag (1958).

TABLE 1

RESULTS OF CALIBRATION TESTS TO DETERMINE
FRINGE CONSTANTS FOR HOMALITE CR-39

LOT NUMBER (a)	WHITE LIGHT				MONOCHROMATIC LIGHT			
	TENSION		BENDING		TENSION		BENDING	
	With Red Filter	Without Red Filter	With Red Filter	Without Red Filter	With Red Filter	Without Red Filter	With Red Filter	Without Red Filter
1		84.24	91.52	83.25		83.86	86.53	82.63
2							105.57	92.03

Note:

A. Two different lots of material were used in the program.

TABLE 2

Dimensions of CR-39 Specimens Used for Photoelastic Experiments

Specimen Number	K_t (a) (Notch)	D (in)	d (in)	t (in)	r (in)	Specimen Type (b)	Configuration (see Fig. 3)
A-1	3.0	2.500	1.755	0.252	0.125	I	Specimen contained
B-1	5.2	2.500	1.754	0.255	0.035	I	edge notches
C-1	7.1	2.498	1.754	0.265	0.018	I	only - no
D-1	9.8	2.500	1.754	0.259	0.009	I	holes
E-1	14.2	2.498	1.754	0.257	0.004	I	
A-2	3.0	2.500	1.746	0.253	0.125	II	Edge notches
B-2	5.2	2.499	1.751	0.256	0.035	II	plus 1 series
C-2	7.1	2.498	1.754	0.255	0.018	II	of 3 holes on
D-2	9.8	2.498	1.754	0.267	0.009	II	line between
E-2	14.2	2.499	1.750	0.266	0.004	II	notch roots
A-3	3.0	2.502	1.755	0.265	0.125	III	Edge notches
B-3	5.2	2.499	1.744	0.256	0.035	III	plus 1 series
C-3	7.1	2.500	1.752	0.262	0.018	III	of 5 holes on
D-3	9.8	2.500	1.754	0.253	0.009	III	line between
E-3	14.2	2.498	1.754	0.259	0.004	III	notch roots
A-4	3.0	2.502	1.743	0.263	0.125	IV	Edge notches
B-4	5.2	2.500	1.755	0.259	0.035	IV	plus 5 series
C-4	7.1	2.499	1.754	0.253	0.018	IV	of holes; 3
D-4	9.8	2.499	1.755	0.259	0.009	IV	holes on line
E-4	14.2	2.494	1.754	0.264	0.004	IV	between notch roots
A-5	3.0	2.498	1.743	0.259	0.125	V	Edge notches
B-5	5.2	2.499	1.752	0.260	0.035	V	plus 7 series
C-5	7.1	2.498	1.754	0.255	0.018	V	of holes; 5 holes
D-5	9.8	2.499	1.750	0.255	0.009	V	on line between
E-5	14.2	2.494	1.753	0.260	0.004	V	notch roots

Notes:

(a) K_t is the calculated theoretical elastic stress concentration factor, based on nominal net section area, obtained from Peterson (Ref. 3)

(b) Notch depth for all notches was 30 percent.

TABLE 3

Results of Photoelastic Experiments on CR-39 in Tension at Applied Load of 105 lbs.

Observed Fringe Order (n)	Corresponding Shear Stress 2τ (psi)	Fringe Location - (in) (a) Specimen Number				
		A-1	B-1	C-1	D-1	E-1
Edge of spec.	-	0.878	0.872	0.877	0.879	0.878
3	1104	-	0.864	0.870	0.873	-
2	736	0.862	0.858	0.866	0.869	0.870
1	368	0.839	0.848	0.860	0.864	0.867
Center of spec.	0	0	0	0	0	0
		A-2	B-2	C-2	D-2	E-2
Edge of spec.	-	0.873	0.876	0.877	0.877	0.877
3	999	-	0.864	-	-	-
2	666	0.856	0.860	0.863	0.872	0.871
1	333	0.829	0.848	0.857	0.866	0.868
1	333	0.518	0.519	0.518	0.522	0.524
hole	-	hole	hole	hole	hole	hole
1	333	0.404	0.403	0.406	0.407	0.409
1	333	0.057	0.057	0.317	0.058	0.353
Center of spec.	-	0	0	0	0	0
		A-3	B-3	C-3	D-3	E-3
Edge of spec.	-	0.878	0.872	0.876	0.877	0.878
3	1104	0.874	-	-	0.871	-
2	736	0.862	0.862	0.866	0.867	0.872
1	368	0.839	0.846	0.859	0.863	0.867
1	368	0.672	0.671	0.671	0.669	0.672
hole	-	hole	hole	hole	hole	hole
1	368	0.555	0.556	0.557	0.554	0.556
1	368	0.364	0.364	0.363	0.363	0.365
hole	-	hole	hole	hole	hole	hole
1	368	0.252	0.251	0.251	0.250	0.252
1	368	0.057	0.057	0.056	0.056	0.057
Center of spec.	-	0	0	0	0	0

Note:

(a) The location of fringes was measured in the transverse direction from the centerline of the specimens.

TABLE 4

Results of Photoelastic Experiments on CR-39 in Tension at Applied Load of 105 lbs.

Observed Fringe Order (n)	Corresponding Shear Stress 2τ (psi)	Fringe Location - (in) (a) Specimen Number				
		A-4	B-4	C-4	D-4	E-4
Edge of spec.	-	0.862	(b) Test	0.877	0.878	0.877
2	666	0.853	not	0.865	0.872	0.869
1	333	0.824	valid	0.858	0.867	0.865
1	333	0.523	|	0.517	0.523	0.518
hole	-	hole	hole	hole	hole	hole
1	333	0.399	|	0.397	0.399	0.400
1	333	0.057	↓	0.060	0.061	0.060
Center of spec.	-	0	0	0	0	0
		A-5	B-5	C-5	D-5	E-5
Edge of spec.	-	0.872	0.876	(b) Test	(b) Test	0.877
3	999	-	0.866	not	not	0.875
2	666	0.852	0.860	valid	valid	0.870
1	333	0.832	0.849	|	|	0.869
1	333	0.669	0.670	|	|	0.672
hole	-	hole	hole	hole	hole	hole
1	333	0.552	0.550	|	|	0.552
1	333	0.363	0.363	|	|	0.364
hole	-	hole	hole	hole	hole	hole
1	333	0.246	0.248	|	|	0.247
1	333	0.063	0.058	↓	↓	0.060
Center of spec.	-	0	0	0	0	0

Notes:

(a) The location of fringes was measured in the transverse direction from the centerline of the specimens.

(b) Specimens were found to have small cracks at the notch root before testing.

TABLE 5

Results of Photoelastic Experiments on CR-39 in Tension at Applied Load of 157.7 lbs.

Observed Fringe Order (n)	Corresponding Shear Stress 2τ (psi)	Fringe Location - (in) (a) Specimen Number				
		A-1	B-1	C-1	D-1	E-1
Edge of spec.	-	0.878	0.872	0.877	0.879	0.878
4	1472	-	0.863	-	-	0.872
3	1104	0.861	0.858	0.866	0.872	0.867
2	736	0.845	0.851	0.860	0.869	-
1	368	0.800	0.837	0.847	0.864	0.865
Center of spec.	-	0	0	0	0	0
		A-2	B-2	C-2	D-2	E-2
Edge of spec	-	0.873	0.876	0.877	0.877	0.877
3	999	0.861	0.860	0.866	0.869	0.868
2	666	0.847	0.852	0.861	0.866	0.865
1	333	0.809	0.838	0.852	0.858	0.864
1	333	0.525	0.523	0.523	0.527	0.527
2	666	0.515	-	-	-	-
hole	-	hole	hole	hole	hole	hole
2	666	0.410	-	-	-	-
1	333	0.400	0.400	0.400	0.399	0.398
1	333	0.063	0.058	0.058	0.064	0.062
2	666	0.052	-	-	-	-
Center of spec.	-	0	0	0	0	0

Note:

(a) The location of fringes was measured in the transverse direction from the centerline of the specimens.

TABLE 6

Results of Photoelastic Experiments of CR-39 in Tension at Applied Load of 157.7 lbs.

Observed Fringe Order (n)	Corresponding Shear Stress 2τ (psi)	Fringe Location --(in) (a) Specimen Number				
		A-3	B-3	C-3	D-3	E-3
Edge of spec.	-	0.878	0.872	0.876	0.877	0.878
3	1104	0.865	0.858	0.867	0.868	0.872
2	736	0.851	0.853	0.861	0.864	0.869
1	368	0.812	0.837	0.857	0.858	0.867
1	368	0.679	0.682	0.675	0.676	0.679
2	736	-	0.666	-	0.665	-
hole	-	hole	hole	hole	hole	hole
2	736	-	0.560	-	0.560	-
1	368	0.633	0.549	0.551	0.549	0.551
1	368	0.370	0.370	0.367	0.367	0.371
2	736	-	0.356	-	0.356	-
hole	-	hole	hole	hole	hole	hole
2	736	-	0.256	-	0.254	-
1	368	0.243	0.242	0.246	0.242	0.245
1	368	0.062	0.063	0.060	0.061	0.063
Center of spec.	-	0	0	0	0	0
		A-4	B-4	C-4	D-4	E-4
Edge of spec.	-	0.862	(b) Test	0.877	0.878	0.877
4	1332	-	not	0.868	0.872	-
3	999	0.850	valid	0.865	0.869	0.873
2	666	0.830	|	0.860	0.867	0.870
1	333	0.788	|	0.851	0.860	0.868
1	333	0.529	|	0.524	0.529	0.527
2	666	-	|	0.510	0.514	-
hole	-	hole	hole	hole	hole	hole
2	666	-	|	0.403	0.404	-
1	333	0.389	|	0.391	0.392	0.394
1	333	0.064	|	0.069	0.068	0.051
2	666	-	↓	0.055	0.054	-
Center of spec.	-	0	0	0	0	0

Notes:

(a) The location of fringes was measured in the transverse direction from the specimen centerline.

(b) Specimen had small cracks at notch root before testing.

TABLE 7

Results of Photoelastic Experiments of CR-39 in Tension at Applied Loads of 157.7 lbs.

Observed Fringe Order (n)	Corresponding Shear Stress 2τ (psi)	Fringe Location - (in) (a) Specimen Number				
		A-5	B-5	C-5	D-5	E-5
Edge of spec.	-	0.872	0.876	(b)Test	(b)Test	0.877
4	1332	-	0.864	not	not	0.871
3	999	0.859	0.859	valid	valid	0.868
2	666	0.842	0.852	|	|	0.866
1	333	0.802	0.838	|	|	0.864
1	333	0.682	0.679	|	|	0.672
2	666	0.667	0.665	|	|	0.665
hole	-	hole	hole	hole	hole	hole
2	666	0.558	0.555	|	|	0.556
1	333	0.542	0.540	|	|	0.544
1	333	0.372	0.372	|	|	0.371
2	666	0.360	0.358	|	|	0.359
hole	-	hole	hole	hole	hole	hole
2	666	0.252	0.252	|	|	0.254
1	333	0.239	0.238	|	|	0.240
1	333	0.071	0.065	|	|	0.067
2	666	0.058	0.055	↓	↓	0.055
Center of spec	-	0	0	0	0	0

Notes:

(a) The location of fringes was measured in the transverse direction from the specimen centerline.

(b) Specimen had small cracks at the notch root before testing.

TABLE 8

RESULTS OF TENSILE TESTS ON CR-39

SPECIMEN NUMBER	FRACTURE LOAD (a) (LBS)	NOMINAL NET SECTION AREA A (IN^2)	FRACTURE STRESS (LB/IN^2) BASED ON A	ACTUAL NET SECTION AREA A^1 (IN^2)	FRACTURE STRESS (LB/IN^2) BASED ON A^1	K_t
A-1	1430	0.442	3230(b)	-	-	3.00
A-2	837	0.442	1890(b)	0.371	2260(b)	3.00
A-3	1092	0.465	2350(b)	0.341	3200(b)	3.00
A-4	990	0.458	2160	0.385	2570	3.00
A-5	910	0.451	2020(d)	0.340	2680(d)	3.00
B-1	995	0.445	2240(b)	-	-	5.23
B-2	1025	0.448	2290	0.376	2730	5.23
B-3	725	0.446	1630(b)	0.326	2220	5.23
B-4	485	0.455	1070(e)	0.382	1270(e)	5.23
B-5	870	0.456	1910	0.334	2600	5.23
C-1	1307	0.465	2810(b)	-	-	7.12
C-2	760	0.447	1700	0.376	2020	7.12
C-3	1100	0.459	2400(b)	0.336	3270(b)	7.12
C-4	835	0.444	1880	0.373	2240	7.12
C-5	575	0.447	1290(e)	0.328	1750(e)	7.12
D-1	835	0.455	1840(b)	-	-	9.83
D-2	645	0.468	1380	0.393	1640	9.83
D-3	900	0.444	2030	0.325	2770	9.83
D-4	826	0.455	1820	0.382	2160	9.83
D-5	440	0.446	990(e)	0.327	1350	9.83
E-1	685	0.452	1520	-	-	14.15
E-2	625	0.466	1340	0.391	1600	14.15
E-3	675	0.454	1490	0.333	2030	14.15
E-4	485	0.463	1050	0.389	1250	14.15
E-5	710	0.456	1560	0.334	2130	14.15
S-1	600	0.123	4870(d)			
S-2	590	0.125	4730(d)			
S-3	2950	0.610	4840(d)			
S-4	3257	0.687	4740(d)			

Note:

(a) CROSSHEAD SPEED WAS 0.005 IN/MIN

(b) TEST PERFORMED IN SPECIAL TENSILE FIXTURE

(c) K_t IS THE CALCULATED STRESS CONCENTRATION FACTOR BY USING NOMINAL NET SECTION AREA (BASED ON PETERSON'S TABLE)

(d) SPECIMEN DID NOT FAIL AT THE SMALLEST NET SECTION AREA

(e) SPECIMENS HAD SMALL CRACKS AT THE ROOT OF THE NOTCHES BEFORE TESTING

TABLE 9

RESULTS OF TENSILE TESTS ON SHEET SPECIMENS OF
Ti-2.5Al-16V AGED TO A BRITTLE CONDITION

SPECIMEN NUMBER	FRACTURE LOAD (a) (LBS)	NOMINAL NET SECTION AREA A (IN^2)	FRACTURE STRESS BASED ON A (KSI)	ACTUAL NET SECTION AREA A^1 (IN^2)	FRACTURE STRESS BASED ON A^1 (KSI)	ξ_o (b) (in)
T-1	2080	0.0595	35.0	0.0527	39.5	0.011
T-2	2100	0.0595	35.3	0.0527	39.8	0.025
T-3	2355	0.0595	39.6	0.0527	44.7	0.150

Note:
(a) CROSSHEAD SPEED WAS 0.007 IN/MIN
(b) DISTANCE BETWEEN THE ROOT OF THE NOTCH AND THE EDGE OF THE SMALL HOLE

TABLE 10

LONGITUDINAL TENSILE STRESS σ_y CALCULATED FROM

$$\sigma_y = K_t \cdot \sigma_N \sqrt{\frac{r}{r + 4x}} \qquad \text{(PSI)}$$

K_t	SPECIMEN NUMBER	σ_Y (PSI) FOR APPLIED LOAD OF 157.7 LBS. DISTANCES FROM ROOT OF THE NOTCH (IN)			
		x = o	x = 0.010	x = 0.030	x = 0.060
3	A-1	1270	1100	900	740
5.23	B-1	1850	1260	870	650
7.12	C-1	2410	1330	870	630
9.83	D-1	3410	1430	890	650
14.15	E-1	5030	1560	860	600

K_t = THEORETICAL ELASTIC STRESS CONCENTRATION FACTOR

$\sigma_n = \frac{P}{A}$ where P = APPLIED TENSILE LOAD

A = MINIMUM CROSS SECTION AREA

r = RADIUS AT NOTCH ROOT

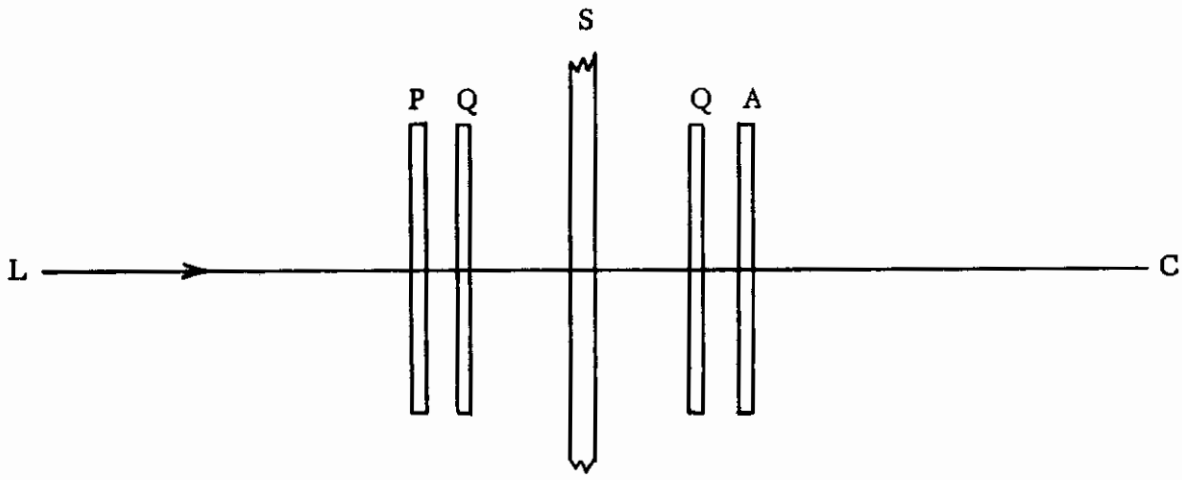

L = LIGHT SOURCE
GE - SUNLAMP 275W, 110V, 60 CPS
P = POLARIZER
A = ANALYZER
Q = QUARTER WAVE PLATE
C = CAMERA
S = SPECIMEN

FIG. 1 TRANSMISSION POLARISCOPE SYSTEM USED FOR PHOTOELASTIC EXPERIMENTS

TENSILE SPECIMEN:

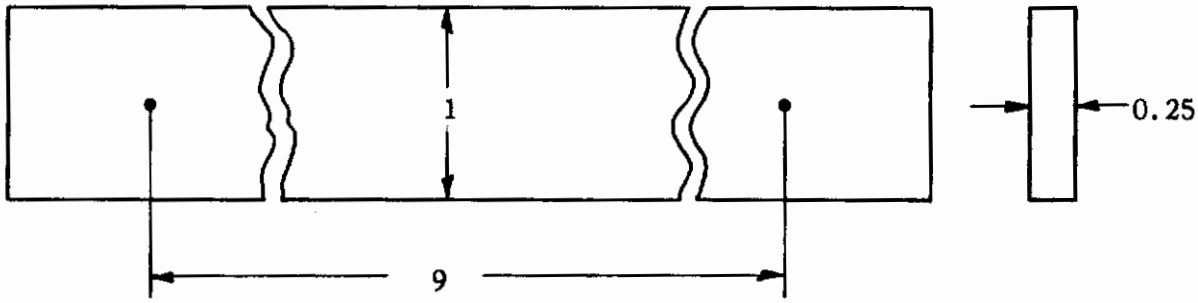

NOTE: ALL DIMENSIONS ARE GIVEN IN INCHES

BEND SPECIMEN:

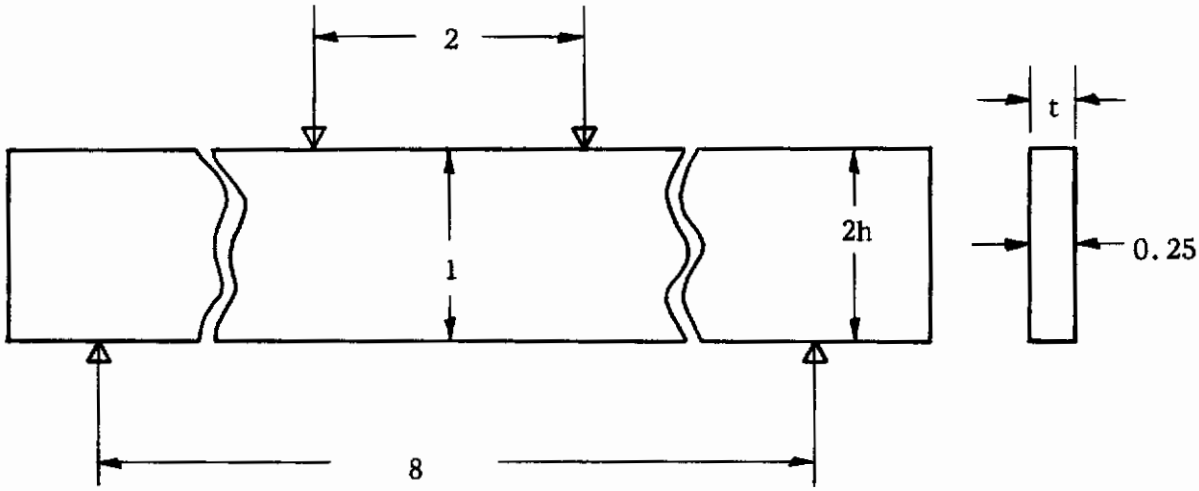

FIG. 2 DESIGN OF TENSILE AND BEND SPECIMENS USED FOR CALIBRATION TESTS ON CR-39

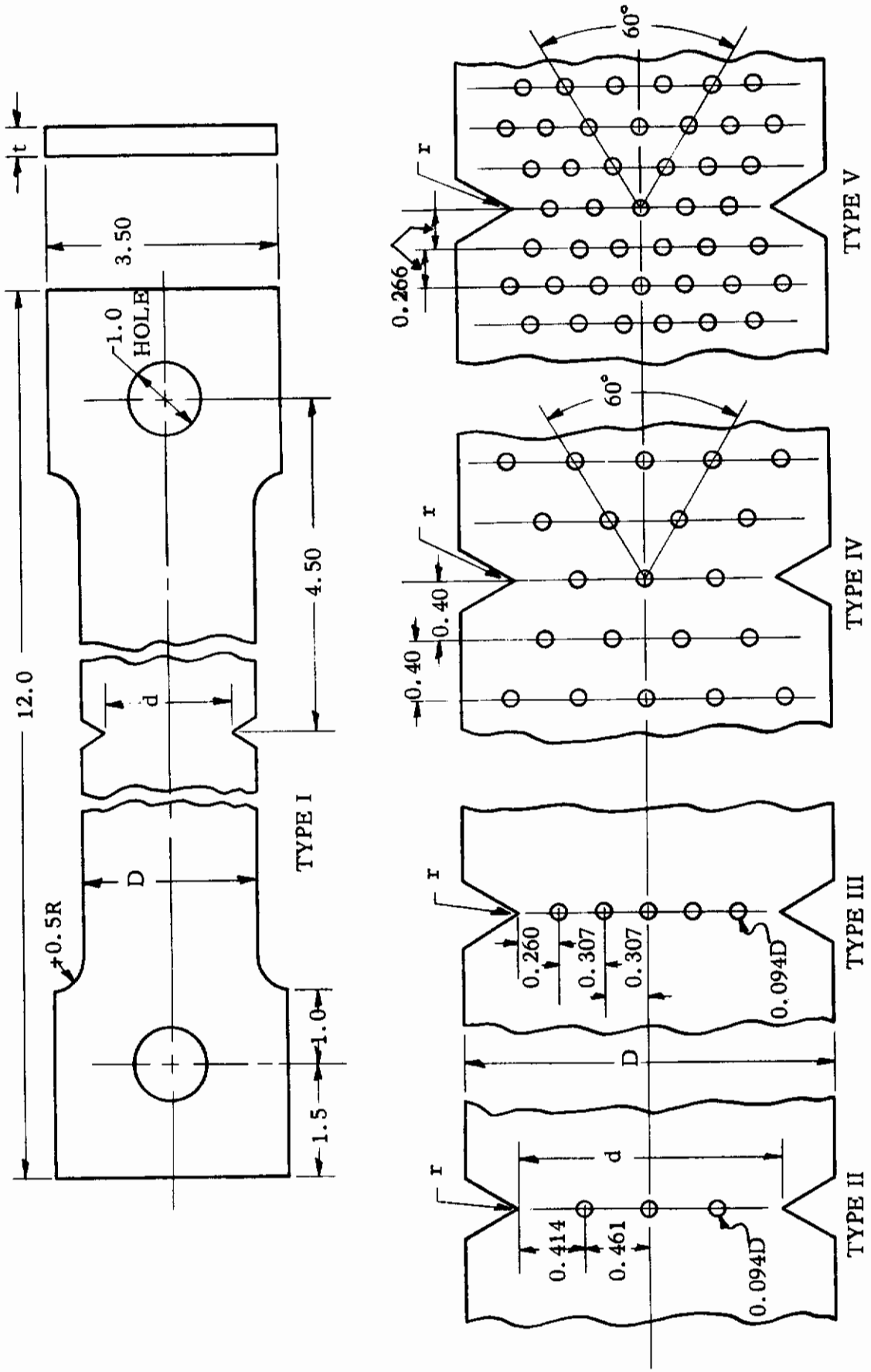

FIG. 3 DESIGN OF SHEET SPECIMENS USED FOR PHOTOELASTIC STUDIES ON CR-39

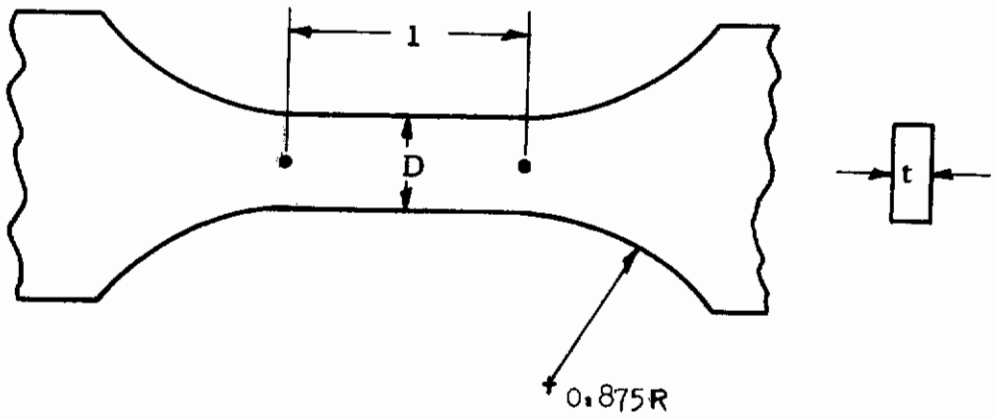

SPECIMEN NUMBER	D (in)	t (in)
S-1	.499	.246
S-2	.505	.247

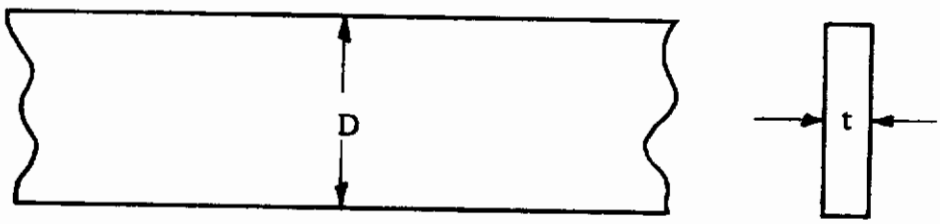

SPECIMEN NUMBER	D (in)	t (in)
S-3	2.522	.242
S-4	2.715	.253

FIG. 4 SPECIMEN DESIGN FOR SMOOTH TENSILE TESTS ON CR-39

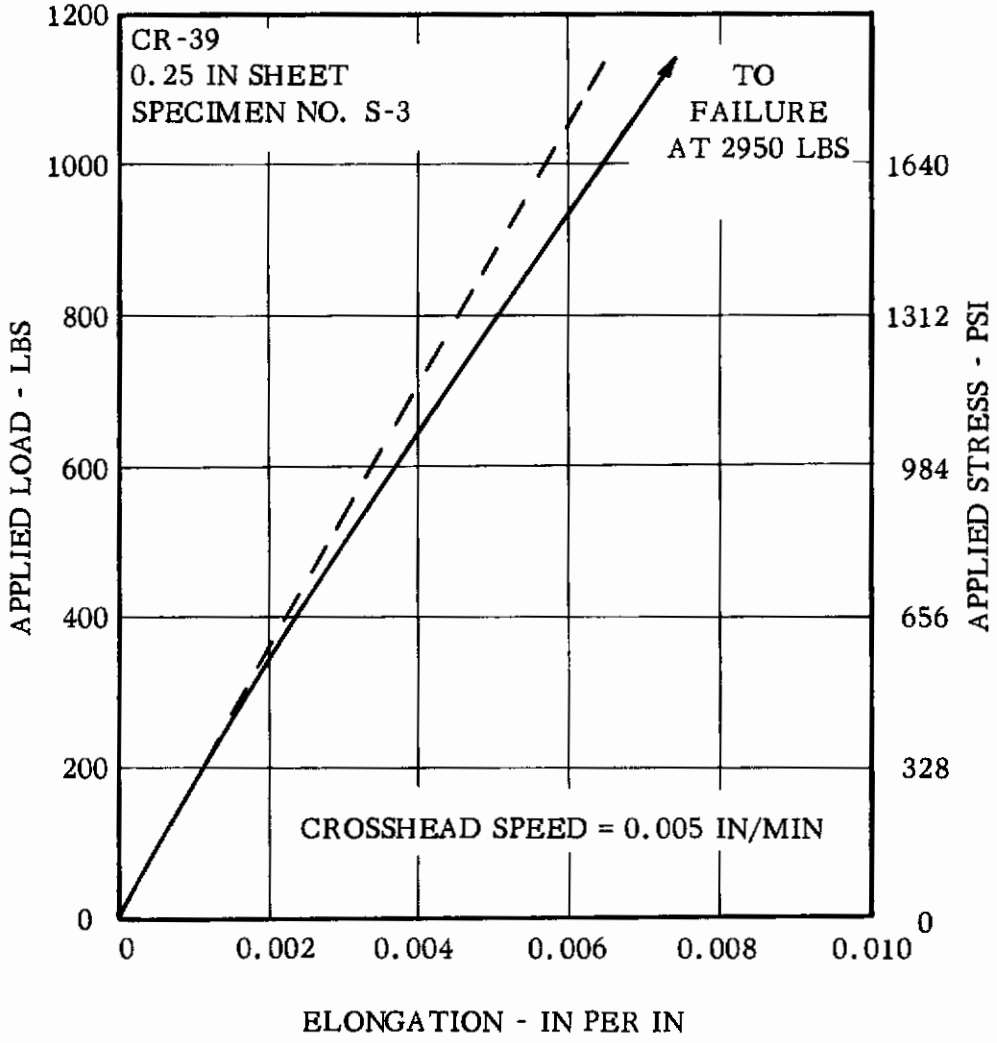

FIG. 5 LOAD-ELONGATION CURVE FOR SMOOTH SPECIMEN OF CR-39 IN TENSION

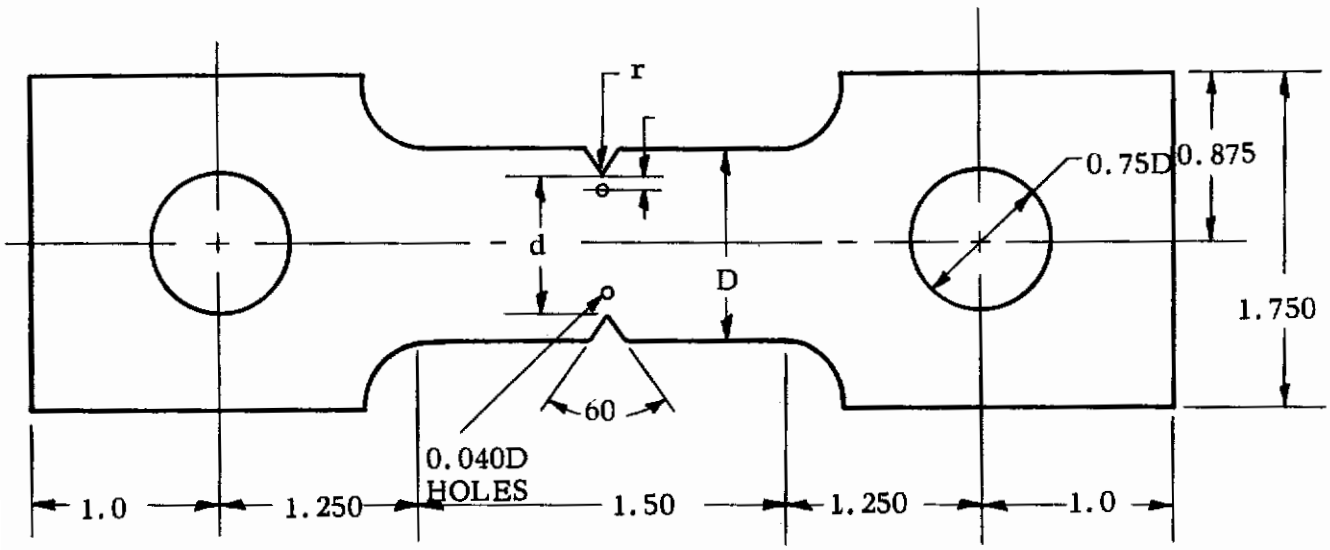

SHEET THICKNESS (t) = 0.085

SPECIMEN NUMBER	D (in)	d (in)	r (in)	ξ (in)	K_t
T-1	1	0.7	0.025	0.011	4.0
T-2	1	0.7	0.025	0.025	4.0
T-3	1	0.7	0.025	0.150	4.0

FIG. 6 DESIGN OF NOTCH TENSILE SPECIMEN USED FOR FRACTURE TESTS ON Ti-2.5Al-16V SHEET

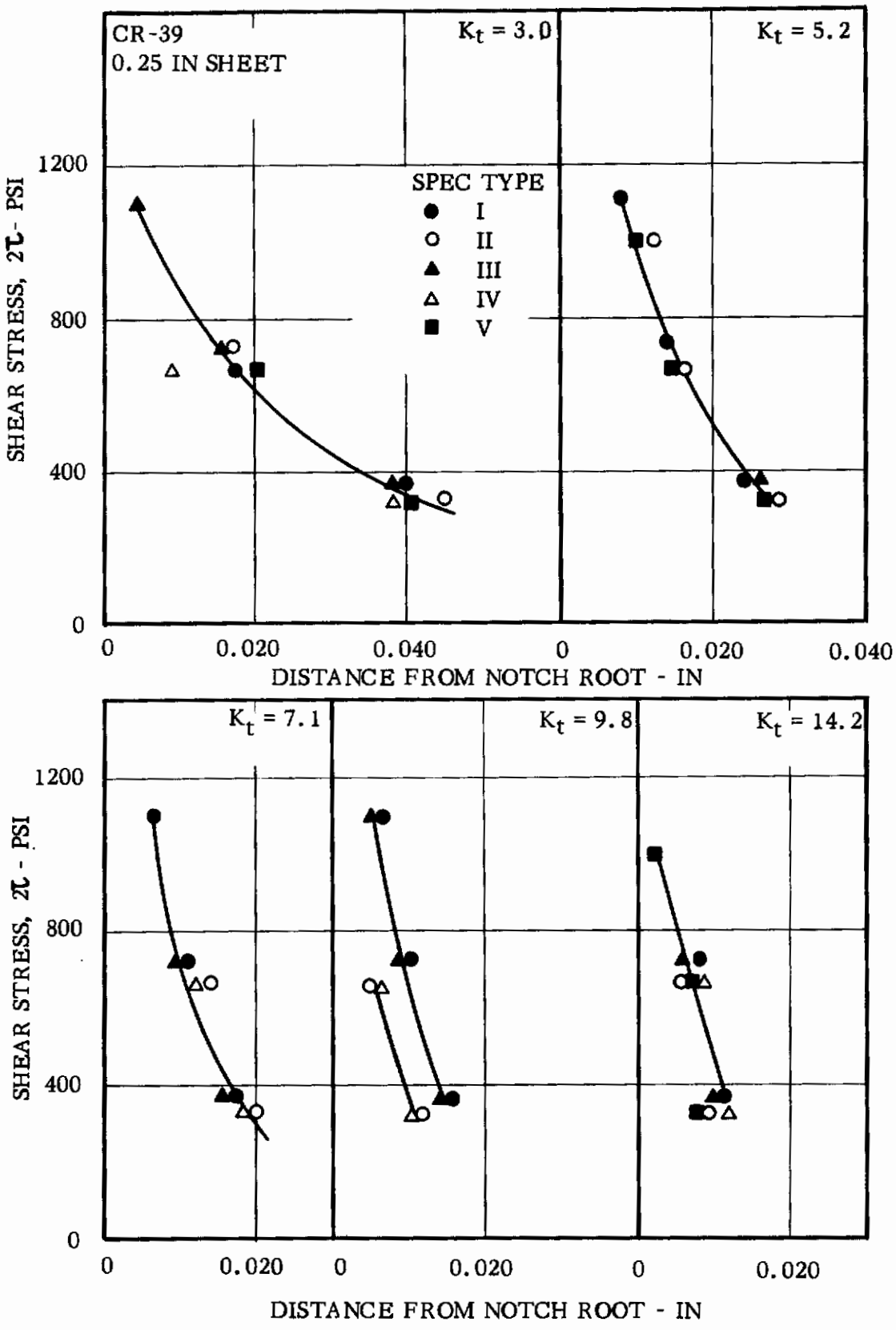

FIG. 7 RESULTS OF SHEAR STRESS DISTRIBUTION MEASUREMENTS FOR THE VARIOUS TYPES OF SPECIMENS AT APPLIED LOAD OF 105 LBS

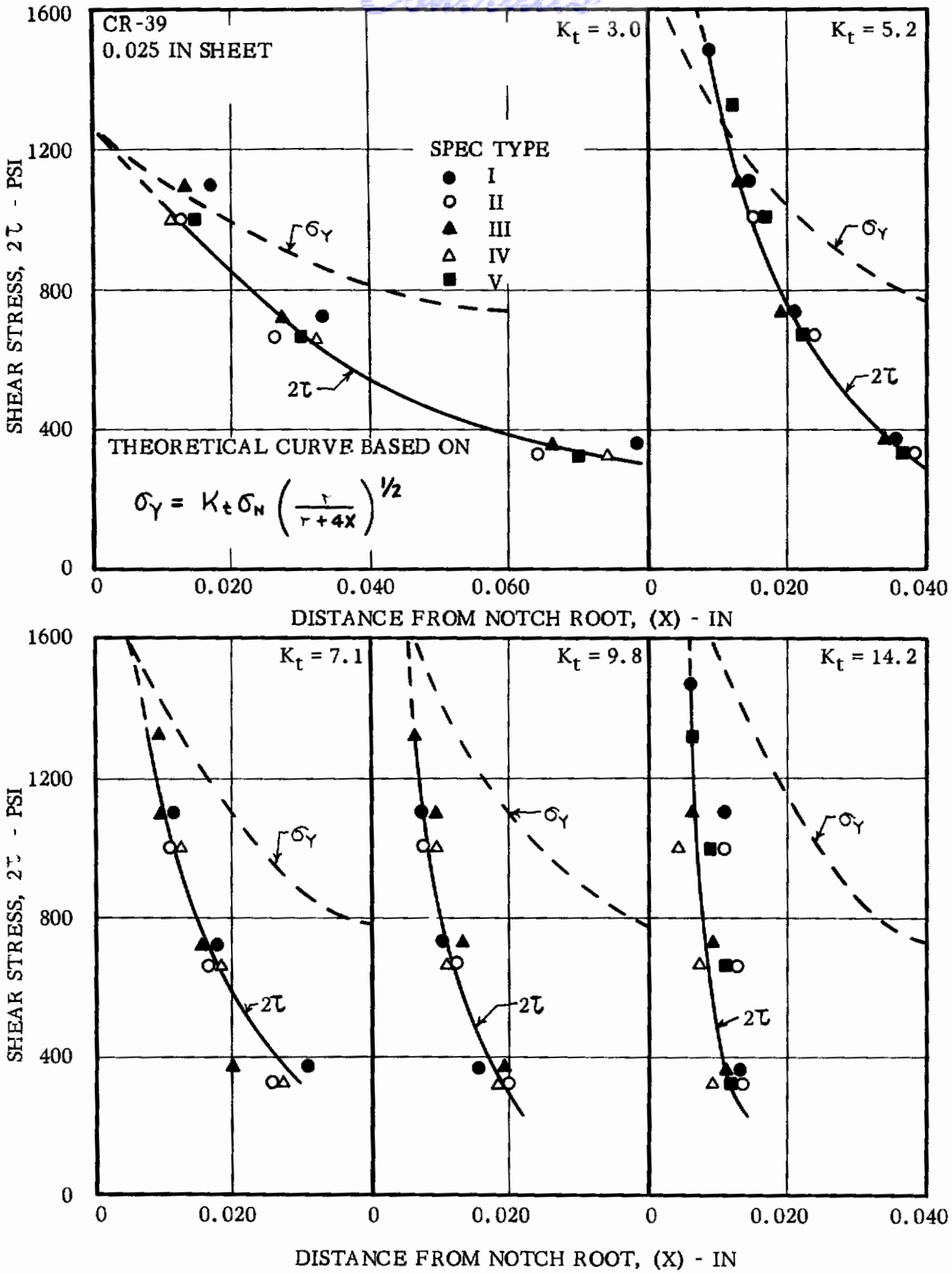

FIG. 8 COMPARISON OF SHEAR STRESS DISTRIBUTION MEASUREMENTS FOR THE VARIOUS TYPES OF SPECIMENS AT APPLIED LOAD OF 157.7 LBS TO THEORETICAL CURVES

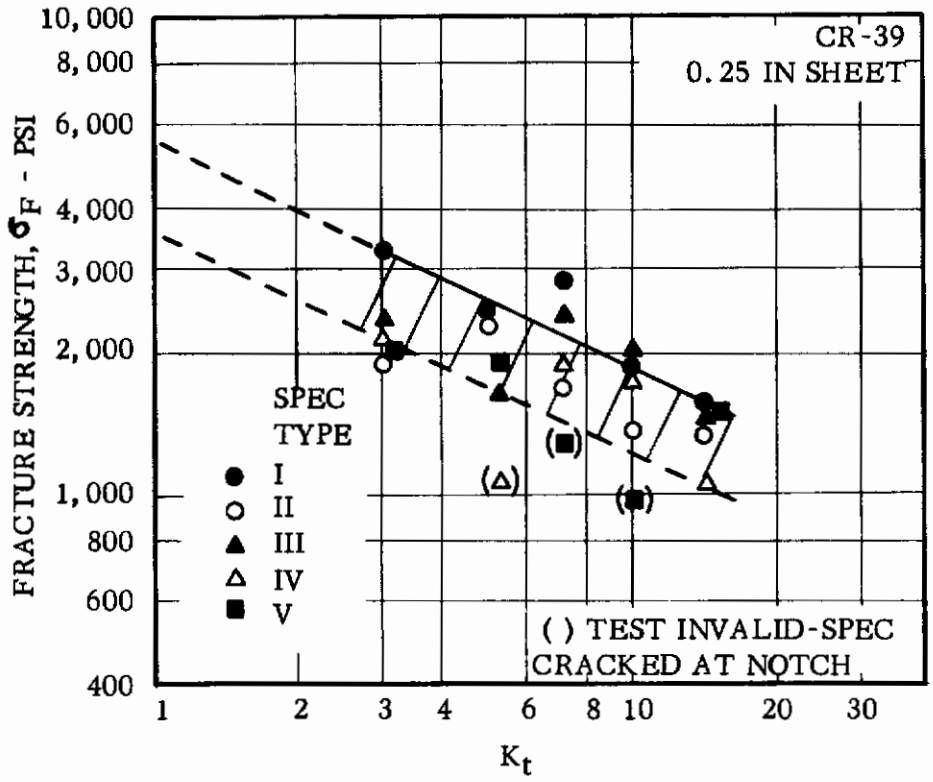

FIG. 9 RESULTS OF NOTCHED TENSILE TESTS ON THE VARIOUS TYPES OF SPECIMENS OF CR-39 SHEET

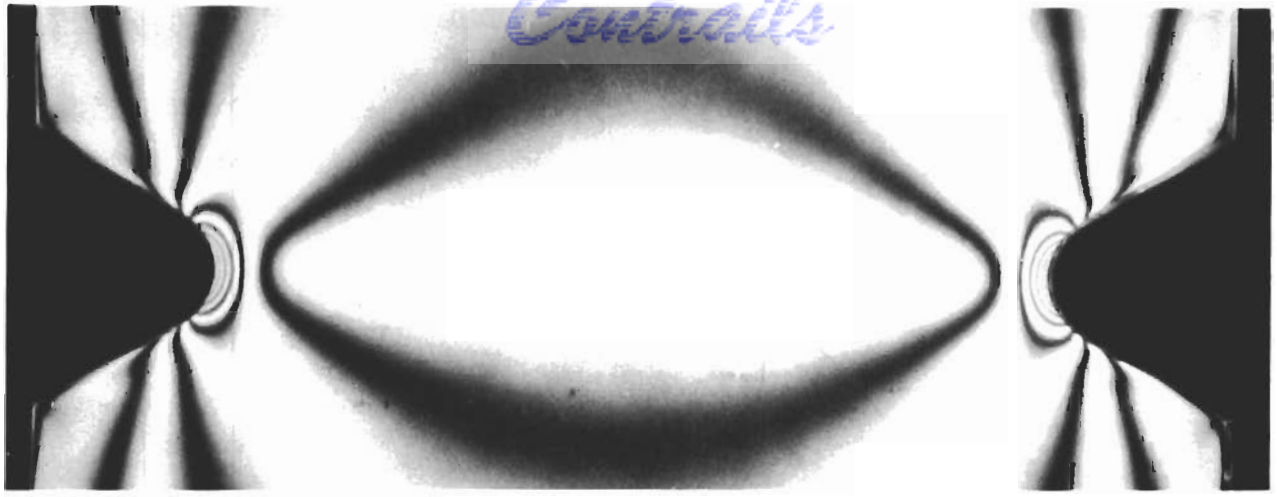

TYPE I

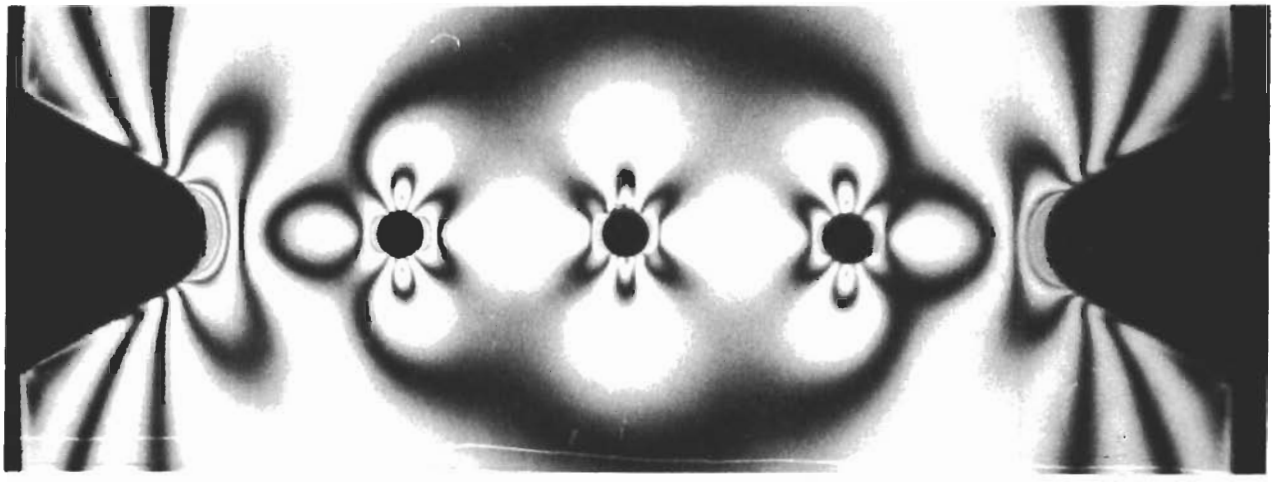

TYPE II

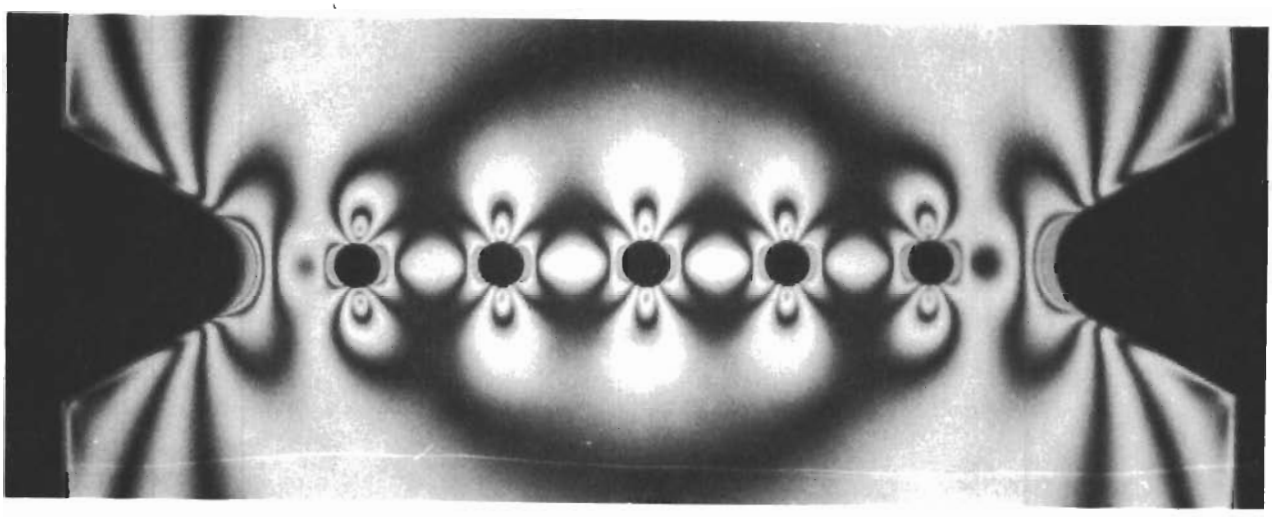

TYPE III

FIG. 10 ISOCHROMATIC PATTERNS OF CR-39 NOTCH SPECIMEN (K_t=3) FOR SPECIMEN TYPES I, II AND III UNDER TENSILE LOAD OF 420 LBS.

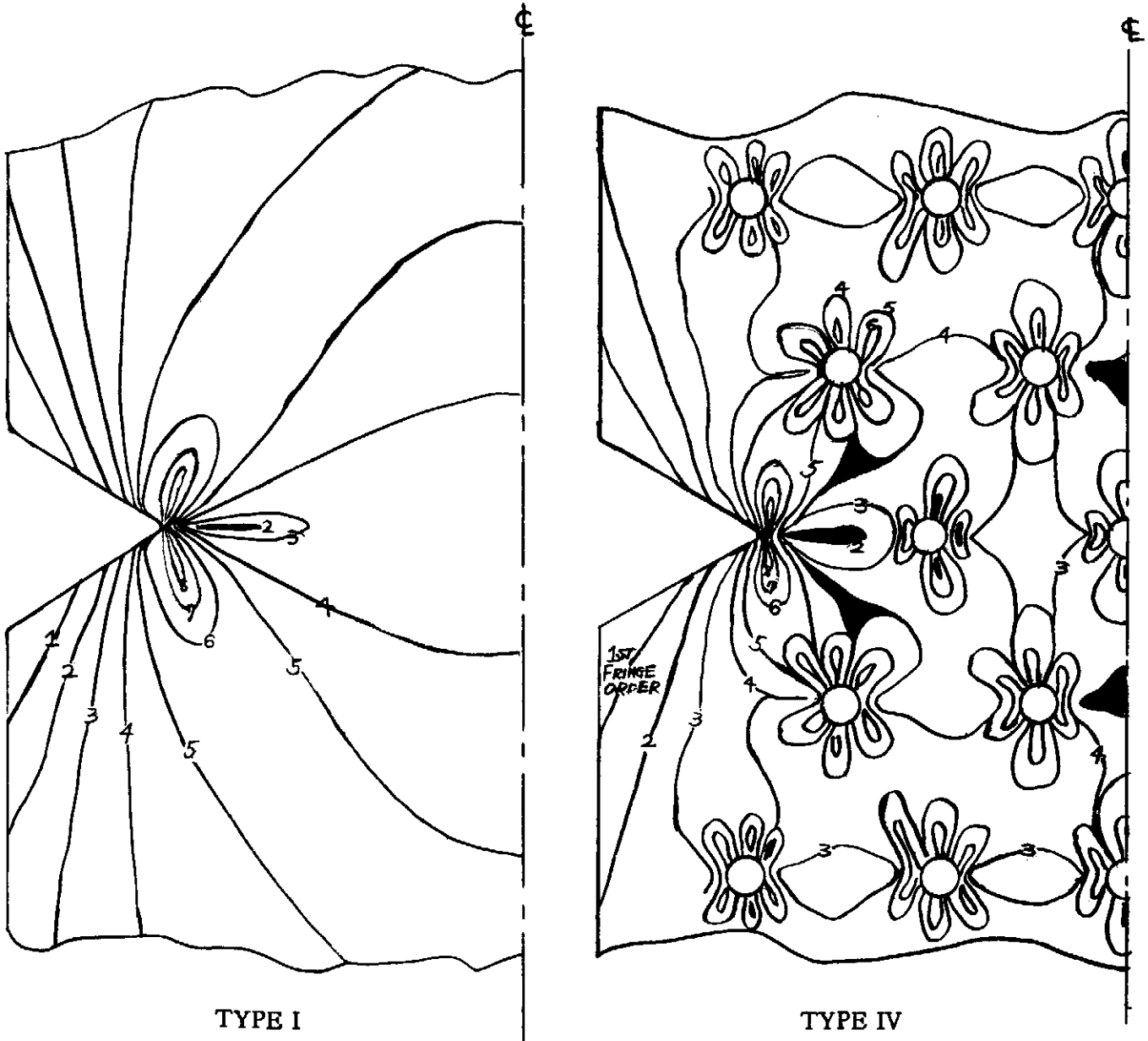

FIG. 11 SKETCHES OF ISOCHROMATIC FRINGE PATTERNS TRACED FROM PHOTOGRAPHS OF SPECIMEN TYPES I AND IV TAKEN JUST PRIOR TO FAILURE

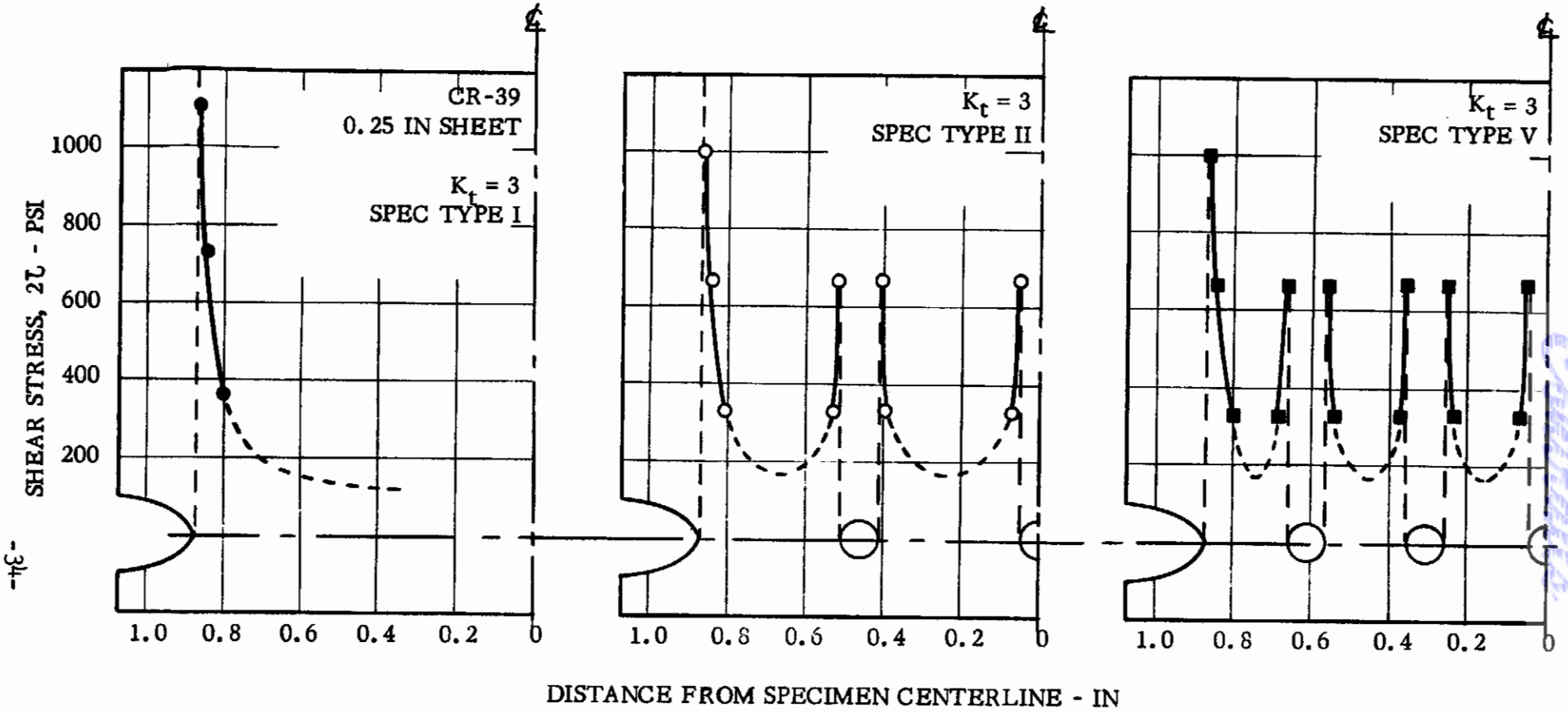

FIG. 12 SHEAR STRESS DISTRIBUTION FROM NOTCH ROOT TO SPECIMEN CENTERLINE FOR THREE SPECIMEN TYPES (K_t = 3) AND APPLIED LOAD = 157.7 LBS